The part of the solar spectrum with the highest influence on the formation of SOA in the continental boundary layer

M. Boy, M. Kulmala

Atmos. Chem. Phys., 2, 375–386, 2002
www.atmos-chem-phys.org/acp/2/375/

Atmospheric Chemistry and Physics

The part of the solar spectrum with the highest influence on the formation of SOA in the continental boundary layer

M. Boy and M. Kulmala

Dept. of Physical Sciences, University of Helsinki, P.O. Box 64, FIN-00014, UHEL, Finland

Received: 25 April 2002 – Published in Atmos. Chem. Phys. Discuss.: 9 September 2002
Revised: 14 November 2002 – Accepted: 15 November 2002 – Published: 28 November 2002

Abstract. The relationship between nucleation events and spectral solar irradiance was analysed using two years of data collected at the Station for Measuring Forest Ecosystem-Atmosphere Relations (SMEAR II) in Hyytiälä, Finland. We analysed the data in two different ways. In the first step we calculated ten nanometer average values from the irradiance measurements between 280 and 580 nm and explored if any special wavelengths groups showed higher values on event days compared to a spectral reference curve for all the days for 2 years or to reference curves for every month. The results indicated that short wavelength irradiance between 300 and 340 nm is higher on event days in winter (February and March) compared to the monthly reference graph but quantitative much smaller than in spring or summer. By building the ratio between the average values of different event classes and the yearly reference graph we obtained peaks between 1.17 and 1.6 in the short wavelength range (300–340 nm). In the next step we included number concentrations of particles between 3 and 10 nm and calculated correlation coefficients between the different wavelengths groups and the particles. The results were quite similar to those obtained previously; the highest correlation coefficients were reached for the spectral irradiance groups 3–5 (300–330 nm) with average values for the single event classes around 0.6 and a nearly linear decrease towards higher wavelengths groups by 30%. Both analyses indicate quite clearly that short wavelength irradiance between 300 and 330 or 340 nm is the most important solar spectral radiation for the formation of newly formed aerosols. In the end we introduce a photochemical mechanism as one possible pathway how short wavelength irradiance can influence the formation of SOA by calculating the production rate of excited oxygen. This mechanism shows in which way short wavelength irradiance can influence the formation of new particles even though the absolute values are one to two magnitudes smaller compared to irradiance between 400 and 500 nm.

Correspondence to: M. Boy (Michael.Boy@helsinki.fi)

1 Introduction

Atmospheric aerosols are amongst other constituents responsible for light scattering, cloud formation and heterogeneous chemical effects and they are a key factor in balancing global climate (e.g. Houghton et al., 1996). There are two main sources for atmospheric aerosols: the emission of particles – natural or anthropogenic – and the gas-to-particle transfer by homogeneous or heterogeneous nucleation of supersaturated vapours. The formation of secondary aerosols has been extensively studied in different environments in the last decades (e.g. free troposphere: Clarke, 1993; marine: Raes et al., 1997; coastal: O'Dowd et al., 1998; continental boundary layer: Kulmala et al., 2001b; Nilsson et al., 2001). Several nucleation mechanisms have been developed in the past few years to explain the observations of particle bursts in the atmosphere. The best understood way up till now is the binary nucleation of H_2SO_4 and H_2O (Kulmala et al., 1998) or the ternary nucleation of H_2O, NH_3 and H_2SO_4 (Korhonen et al., 1999). According to Kulmala et al. (2000) binary nucleation theory is not able to predict the observed nucleation rates in the atmosphere at typical tropospheric sulphuric acid concentrations ($10^5 - -10^7$ cm^{-3}, Weber et al., 1998; Weber et al., 1999). Ternary nucleation, however, gives significantly higher nucleation rates and thus can better predict the formation of new particles at typical tropospheric conditions (ammonia at a level of a few ppt). Kulmala et al. (2000) suggest that nucleation occurs almost everywhere in the atmosphere, at least during the daytime and leads to a reservoir of thermodynamically stable clusters (TSCs), which under certain conditions grow to detectable sizes. However we still do not exactly know under what kind of meteorological and physical conditions the growth of these TSCs will occur and which precursor gases are necessary.

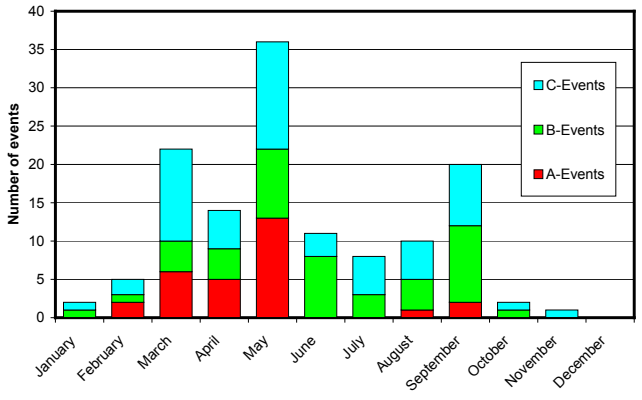

Fig. 1. Monthly distribution of event classes for 2000 and 2001.

In our last publication (Boy and Kulmala, 2002) we suggested that UVA solar radiation is one key parameter for the formation of new particles. We calculated ratios of UVA to different solar bands (PAR – photo synthetically active radiation, reflected PAR, global, reflected global and net radiation) and plotted these ratios against the number concentrations of particles between 3–5 nm during the time the particle bursts occurred. Our analysis for that work was based on radiation sensor data from 1999. In January 2000 we installed a radiospectrometer – measuring solar irradiance between 280–580 nm – in Hyytiälä and in this experimental series we used continuous measurements made with this instrument to investigate more detailed information about what part of the solar spectrum has the highest influence on the formation of newly formed aerosols.

2 Measurements

Data were collected at the Station for Measuring Forest Ecosystem-Atmosphere Relations (SMEAR II) in Hyytiälä, Finland. The station is located in Southern Finland (61°51′ N, 24°17′ E, 181 m asl), within extended areas of pine-dominated forests. For a detailed description of the SMEAR II station and instrumentation, we refer to Vesala (1998). The conditions at the site are typical for a background location, however, occasionally measurements were polluted by the station buildings (0.5 km) and the city of Tampere (60 km) both located in a west-south-west direction from the instruments.

Nucleation events have been classified into A, B and C classes (Mäkelä et al., 2000) and an extra group (marked by S) for days with small indications that the formation of new particles had occurred but not enough indications to classify the formation as an event. Class A events are categorised by high amounts of 3 nm particles and continuous growth to larger particle sizes. Class B events show the same behaviour with less clarity and class C events are marginal nucleation events where one of the two stages was not clearly observed. This type of classification is quite subjective and takes into account the uncertainties and limitations of the instrumentation. Because of this, there will always exist an overlap between the classes. There are new numerical methods which have been published (Birmili et al., 2001) to classify different event days by the maximal number concentration of particles in the nucleation mode, the background aerosol concentration and the characteristic times for the concentration curves of the newly formed particles increase and decrease.

These methods may have some advantages compared to our technique of looking at all the days and deciding in a more or less subjective way the class of the event. However there are still disagreements in the scientific community about the best way numerical solutions can be used for classification and all numerical methods need to be modulated to the location. For these reasons we used for this work the old classification system for the events. In Table 1 all events of 2000 and 2001 are listed including the start and the end time of the particle bursts and some extra parameters which will be explained later. The monthly distribution of A to C events for 2000 and 2001 (Fig. 1) shows two peaks: the first one in spring (March till May) with 40% of event-days and a second smaller one in autumn (August and September) with 25% of the events.

The spectral solar radiation data were measured using a radiospectrometer system produced by Bentham (England). The system consists of the following four components:

- A DM150 double monochromator with 300 mm focal length, fixed slit, remote operated swing-away mirror, holographic gratings (2400 g/mm blazed at 250), internal 6-position stepping-motor-driven filter wheel, filter set for UV solar measurement (selected for order sorting and optimum stray light detector hysteresis) and an end window pmt bialkali photo cathode
- Benthams 200 series Detection electronics; including the 217-T power supply & display, 215 high voltage power supply, 228A integrating A to D converter and 267 programmable d.c. amplifier
- Input optics; including a ptfe diffuser (200–800 nm) and an UV transmitting fibre optic (2 m, 4 mm dia to 13 × 1 mm)
- Data transfer equipment; including a 488/IEEE interface card for use with a PCMIA expansion socket on a PC, two IEEE/488 Cables, radiospectrometer control and data acquisition, display and manipulation software

The whole system is placed above the tree level in a small wooden cottage on a 10 m high building to insure an undisturbed solar irradiance throughout the year. The diffuser is protected by a quartz-glass which has a high transmittance (94–96%) in the measured wavelength-range and dry air is streaming permanently into the dome to prevent condensation. The calibration of the glass dome is made by measuring

Table 1. Date, start and end time of the particle bursts; Time of the day spectral irradiance (300–339 nm) reaches 600 mW m^{-2}; Time of the day particle concentration (3–10 nm) exceeds 400 particle cm^{-3}; Maximal spectral irradiance (in 300–339 nm) and maxima particle number concentration (in 3–10 nm) for all A- and B-events of 2000 and 2001

Date	Doy	Start of particle burst	End of particle burst	Time at I_{600}	I_{max} [mW m^{-2}] (300–339 nm)	Time at N_{400}	N_{max} [cm^{-3}] (3–10 nm)
A-Events							
20000205	36	9,18	15,41	11,74	628	9,51	2073
20000311	71	9,49	14,95	7,78	4249	10,38	2542
20000312	72	11,21	16,69			11,21	3272
20000329	89	8,69	15,44	6,84	5967	8,43	10848
20000407	98	8,39	14,79	6,47	6066	9,08	2029
20000502	123	10,78	14,79	5,40	7975	10,84	4026
20000504	125	6,95	14,39	5,36	8330	7,10	2885
20000506	127	6,27	15,01	5,18	8520	5,89	3976
20000507	128	9,61	15,56	5,09	8236	9,65	3699
20000508	129	9,00	13,47	5,29	7347	9,37	2433
20000511	132	7,72	17,94	5,50	7898	8,62	2415
20000512	133	6,92	17,92			7,25	8086
20000514	135	9,86	14,82			10,41	1469
20000515	136	11,36	13,17		9051	11,47	1901
20000518	139	7,90	13,90	4,85	8318	7,66	4126
20000921	265	10,90	14,85			11,32	6482
20000926	270	11,36	15,65			11,61	1884
20010216	47	10,96	15,10	9,28	2128	11,33	2743
20010307	66	10,78	15,16			9,64	3846
20010319	78	9,80	16,93	7,50	4422	10,03	7592
20010325	84	10,26	15,34	7,17	5004	10,49	2792
20010403	93	8,27	13,60	6,64	6057	8,35	4859
20010405	95	8,85	12,25	6,69	4939		3320
20010413	103	8,21	18,34			8,47	8453
20010414	104	7,32	13,26			4,96	4128
20010510	130	8,24	13,81	5,06	7478		2712
20010511	131	9,16	14,24	5,07	8975	9,49	2412
20010514	134	10,47	14,39	4,94	8414	10,58	1375
20010828	240	8,70	11,61	6,17	7049	9,01	4056
20000117	17	12,40	16,29			12,86	1303
20000328	88	10,41	15,50	6,91	5440	10,30	2195
20000402	93	11,27	16,26	6,67	6014	12,00	1995
20000423	114	9,43	13,47	5,79	7114	9,46	2261
20000427	118	13,05	14,36	5,75	6693	12,79	1736
20000430	121	9,09	15,34	5,43	8043	9,26	3174
20000501	122	8,50	15,66	5,37	7917	10,80	1149
20000505	126	9,83	13,54	5,44	7979	10,17	1803
20000516	137	7,74	12,43	4,84	9109		1285

solar radiation on cloudless days with and without the glass about twice per year.

The calibration sources include two calibrated Bentham CL6-H lamps (150 W, 250–2500 nm, in a housing with mounting for a direct connection to diffuser), a current stabilised power supply 250 W with automatic current ramp up/down facility and a mercury calibration lamp with a mounting for direct connection to the DM150. The signal calibration is carried out once a month with one of the two CL6-H lamps and once every 3 months the second CL6-H lamp is used as a reference emitter to recalibrate the first lamp if necessary. The wavelengths are checked also once every three months and in the two years a maximum wavelength shift of 0.4 nm at 253.65 nm was detectable.

The spectroradiometer has been making measurements every 30 minutes since 28 January 2000. The scans are from

Table 1. Continued ...

Date	Doy	Start of particle burst	End of particle burst	Time at I_{600} (300–339 nm)	I_{max} [mW m^{-2}]	Time at N_{400} (3–10 nm)	N_{max} [cm^{-3}]
				B-Events			
20000527	148	9,46	16,60	4,60	9498	9,61	1339
20000605	157	7,25	10,44			8,02	753
20000610	162	9,97	13,49	4,36	9844	11,00	986
20000611	163	8,50	11,38	4,49	8646	9,51	884
20000613	165	8,36	12,03	4,28	9645	8,39	1069
20000614	166	9,61	15,44		9907	9,91	1884
20000615	167	7,29	14,55	4,30	10947	8,03	1748
20000617	169	9,55	15,07	4,14	9842	10,05	1734
20000621	173	7,68	12,71	4,27	9632	8,15	1217
20000710	192	9,64	11,67			10,41	447
20000727	209	8,42	14,52	4,95	9475	8,95	2827
20000728	210	11,15	11,97	5,29	5340	11,56	437
20000816	229	10,04	12,16	6,20	7793	10,60	614
20000827	240	10,10	14,92		6163	10,79	2255
20000906	250	10,81	13,38		3838	10,74	1538
20000907	251	10,38	15,10	6,57	5788	10,82	4196
20000910	254	13,05	16,51	6,93	4767	13,21	2044
20000915	259	9,46	15,53	6,90	5522	9,71	1488
20000916	260	11,18	13,11	6,92	5239	11,60	627
20000919	263	12,53	15,65			12,58	3358
20010220	51	9,07	15,49	9,07	2304	9,73	1511
20010308	67	10,96	16,87		3718	12,64	2121
20010317	76	9,04	17,27	7,64	4203	8,94	2398
20010318	77	9,86	16,01	7,64	3679	11,89	1432
20010503	123	9,77	17,70	5,30	8070		9139
20010506	126	9,65	17,54	5,24	8287	10,64	1491
20010513	133	8,06	12,65	5,05	8272	7,81	7531
20010516	136	9,71	16,20	4,91	8432	11,06	1282
20010526	146	9,92	13,04			10,75	741
20010802	214	7,54	14,45	5,21	9221		1276
20010819	231	9,37	14,79	5,84	7542	7,46	1075
20010927	270	9,98	14,73	7,39	4766	9,41	1900
20010928	271	13,29	17,39	7,90	3551	14,08	2390
20010929	272	9,86	17,08			10,27	1012
20010930	273	10,08	16,32			9,82	2787
20011019	292	13,26	16,69	8,89	2293	13,41	1632

280–580 nm and the step-width is 1 nm. The row data are stored and recalibrated afterwards to enable later corrections of the data if necessary.

A Differential Mobility Particle Sizer (DMPS) system (located near the mast) monitors aerosol size distributions at a height of 2 m from ground level giving a continuous view of the distribution and evolution of sub-micrometer aerosol particles. The DMPS system used here actually consists of two components. The first one includes a TSI 3025 UFCPC and a Hauke-type short DMA (Differential Mobility Analyzer) and measures particles between 3 and 20 nm in dry diameter. The second includes a TSI 3010 CPC and a Hauke-type medium DMA capable of measuring particles between 20 and 500 nm. Particle size distribution is recorded every 10 min. A detailed description of this system is given in Jokinen and Mäkelä (1997) and Mäkelä et al. (1997).

Concentrations of ozone were measured with a TEI 49 (Thermo Environmental Instruments) gas analyser based on O_3 specific absorption of UV light. Air samples were collected from the mast at heights of 4.2 m, 16.8 m and 67.2 m every 5 min. Temperature (measured with PT-100-sensors) were collected every 50 s at these three heights as well.

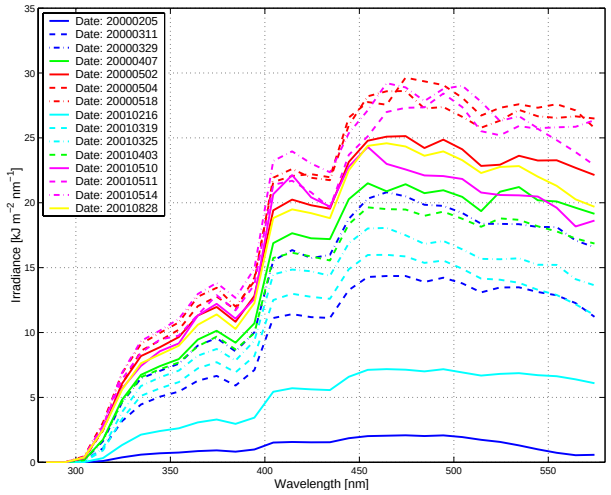

Fig. 2. Spectral solar irradiance for a representative selection of A-event days in 2000 and 2001.

3 Correlation between nucleation and solar spectral irradiance

3.1 Concerning the classification of the events

The importance of solar irradiance for the formation of new particles and the growth of these particles to the Aitken mode has been described in many papers (Birmili and Wiedensohler, 2000; Clement et al., 2000; Kulmala et al., 2001a). However, it is still an open question as to what part of the solar spectrum is responsible for the realization of these processes. To date, nearly all publications have used measurements of global solar irradiance as the radiation parameter. In this work we analysed data from a radiospectrometer measuring solar radiation from 280 to 580 nm with a step width of one nm to gain detailed information about which wavelength range of the solar spectrum has more influence on the formation of new aerosols.

In the first step we divide the measured spectral solar irradiance ISPR into 30 groups with 10 nm wavelength ranges and calculate the average solar irradiance per group per scan per nanometer by

$$I_{S,G}(j,h,d) = \frac{1}{10} \sum_{k=sw(j)}^{ew(j)} I_{SPR}(k,h,d) \qquad (1)$$

with

$$sw(j) = [280, 290, 300, \ldots, 570]\,\text{nm}$$
$$ew(j) = [289, 299, 309, \ldots, 579]\,\text{nm}$$

j is the number of the wavelength groups from 280 to 580 nm, h is the time of the scans starting at 00:00 ending at 23:30 LT (every half hour) and d is the day of the year going form 1 to 731 for 2000 and 2001.

According to our own experience gained from analysing data for two years and the results of Mäkelä et al. (2000) nearly all of the particle bursts occurred between 08:00 and 16:00 LT (see also Table 1). For these reasons in Eq. (2) we calculate the solar energy E_G for each wavelength group and day during this time period.

$$E_G(j,d) = \sum_{h=17}^{32} (I_{S,G}(j,h,d) \cdot 1800) \qquad (2)$$

Figure 2 shows the E_G curves for 15 A-Events in 2000 and 2001 (monthly representative selection). The curves show the same trend but there is a difference of more than one magnitude in all wavelength groups between the highest solar irradiance on 18 May 2000 and 5 February 2000. Although we can produce these plots for all event and non-event days for the two years, the plots will not give us differences in the spectral distribution for different days. Therefore we normalise every day by dividing all wavelengths groups by the mean value of this day between 330 and 380 nm. We then obtain Av, the average of this wavelengths interval, and can then calculate a normalised solar energy EN_G for every day and wavelength group:

$$Av(j,d) = \frac{1}{5} \sum_{j=6}^{10} E_G(j,d)$$
$$EN_G(j,d) = \frac{E_G(j,d)}{Av(j,d)} \qquad (3)$$

The reasons we choose the 330 to 380 nm wavelength interval is the nearly linear trend with different slopes for all these curves throughout the year and the fact that irradiance in this range is mostly diminished by the scattering of permanent gases in the atmosphere and not by water vapour (Seinfeld and Pandis, 1998). In order to compare different event days with all days we now calculate first in Eq. (4) an average normalised spectral solar energy graph.

$$\overline{EN_{G,N}(j)} = \frac{1}{NE} \sum_{d=1}^{NE} EN_G\big(j, N(d)\big) \qquad (4)$$

with the number of all measured days $NE = 546$. The graph of $\overline{EN_{G,N}}$ can now be used as a reference graph of normalised spectral distribution for all days in 2000 and 2001. Now we divide every wavelength group of the A-event days in Fig. 2 with the corresponding values from Eq. (4) by

$$R_A\big(j, A(d)\big) = \frac{EN_G\big(j, A(d)\big)}{\overline{EN_{G,N}(j)}} \qquad (5)$$

The results of Eq. (5) are plotted for all A-events in Fig. 3. The data for wavelengths numbers smaller than 300 nm are uncertain since in this wavelength range we are most of the year at the detection limit of the instrumentation with values smaller than 1 mW m^{-2}. However, we recognise on all

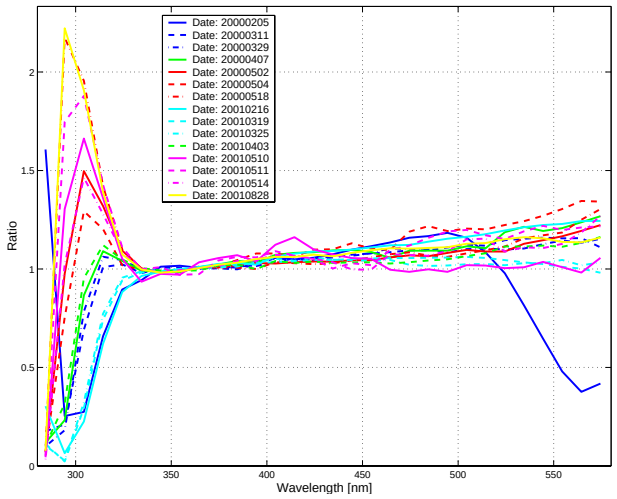

Fig. 3. Ratios for A-events from Fig. 2 of spectral solar irradiance against a yearly reference graph from Eq. (4) ($\overline{E_{G,N}}$).

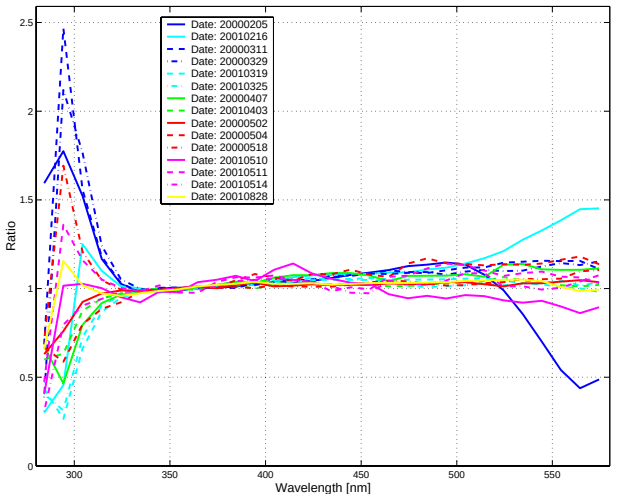

Fig. 4. Ratios for A-events from Fig. 2 of spectral solar irradiance against monthly reference graphs from Eq. (6) ($\overline{E_{G,N,M}}$).

days in April until September (green, red, magenta and yellow curves) a steep rise toward smaller wavelength numbers starting between 330 and 340 nm. This can be equated with an increase in solar radiation by a factor up to 2. On the other side the event days in February and some of the days in March (blue curves) behave in the opposite way with a decrease of spectral irradiance at wavelengths below 340 nm. The right hand side of all the curves are more bunched and mixed than the left side with a weak slope toward higher wavelength numbers. The rest of the A- and B-event days show a similar trend to those in Fig. 3 with a steep increase below 340 nm from April to September and a decrease in the same wavelength range in the autumn and winter months. The reason for this behaviour is physical. In the Finnish autumn and winter the solar zenith angle is always larger than 60° and so the pathway of the solar beam through the atmosphere is much longer compared to summer or spring. Rayleigh scattering is more effective for smaller wavelength than for larger once and this has the consequence that our calculated yearly reference curve is inadequate. To avoid this we calculate by Eq. (6) equal to Eq. (4) and Eq. (5) a spectral solar reference curve for every month and the ratios for every event day to the corresponding month:

$$\overline{EN_{G,N,M}(j,m)} = \frac{1}{MD(m)} \sum_{d=1}^{MD(m)} EN_G\big(j, M(d)\big)$$

$$R_{A,M}\big(j, A(d,m)\big) = \frac{EN_G\big(j, A(d)\big)}{\overline{EN_{G,N,M}(j,m)}} \qquad (6)$$

with MD the amount of measured days per month in 2000 and 2001 (e.g. February = 57). In Fig. 4 the calculated ratios of $R_{A,M}(j, A(d,m))$ are plotted for the A-events of Fig. 2. If we compare this figure now with Fig. 3 we can see that the trend of increasing short wavelength irradiance in spring and summer has disappeared. Further we realise that both events in February and the events in March 2000 show a steep increase in short wavelength radiation in comparison with the reference curve for the corresponding month. The highest increase is by a factor of 2 for the day in March with the smallest amount of solar irradiance (see Fig. 2). We also found that in spring and summer higher and smaller values of spectral radiation between 300 and 340 nm on the event days are well mixed. If we combine the results from Fig. 3 and 4 we can conclude that short wavelength irradiance between 300 and 340 nm is higher on most event days in winter compared to a normalised reference graph for all days of the corresponding month but quantitative still much smaller than in spring or summer. It appears that on days with a low amount of solar energy the relative high values of irradiance between 300 and 340 nm seem to be important. The same results presented here for some of the A-events in 2000 and 2001 can be seen for all the event days. This indicates that for the formation of new particles the responsible solar radiation band is short wavelength irradiance in UV-B and the first 10 to 20 nm of UV-A. We calculate now for all event classes throughout the two years a comprehensive mean value for every wavelength group according to Eq. (4) with NE being now the number of measured event days per class and divide then these values by the values of our reference graph of normalised spectral irradiance for all days in 2000 and 2001 ($\overline{EN_{G,N}}$). The average irradiance per class and the results of the above calculations are shown for all classes in Fig. 5. The amount of solar energy is for A-, B- and C-events in all wavelength groups about 2 times higher compared to the average for all the days in the two years and about 3 times higher compared to the non-event days. The graphs further show an increase in the short wavelength range between 300 to 340 nm and a continuously light increase towards higher wavelengths.

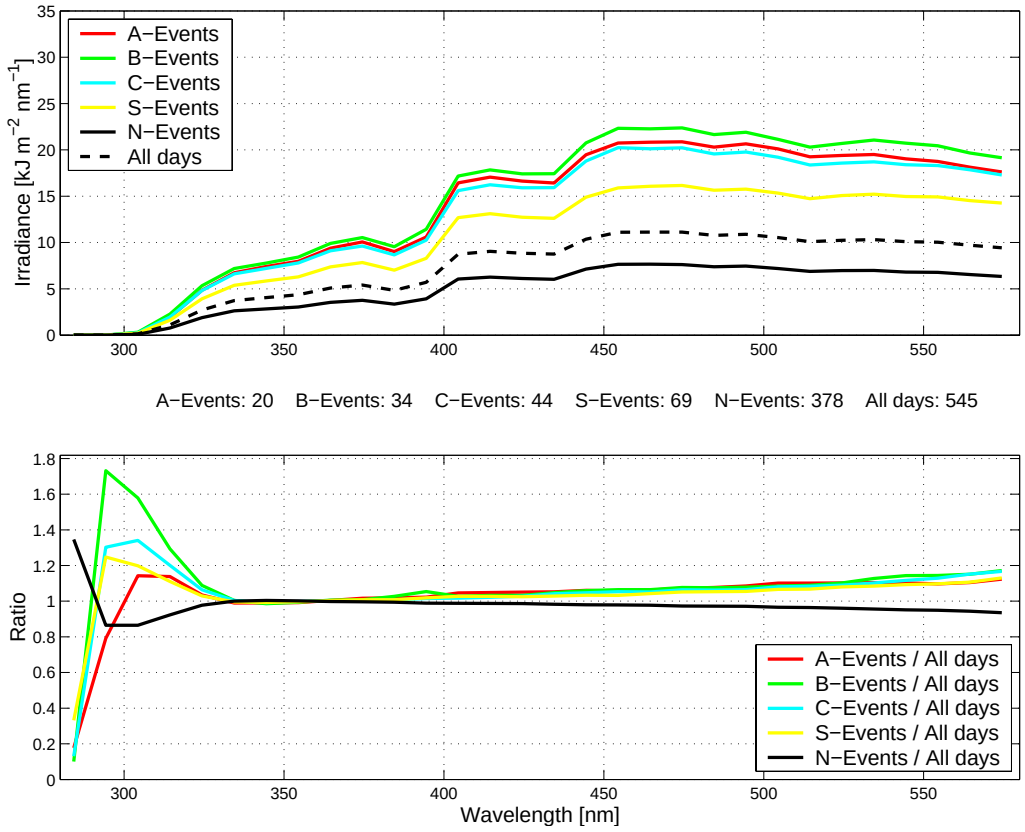

Fig. 5. (a) Average spectral solar irradiance for all event and non-event classes of 2000 and 2001; **(b)** Ratio of the graphs from (a) to a yearly reference graph from Eq. (4) ($\overline{E_{G,N}}$).

3.2 Concerning the number concentration of the particles

So far we have only compared the spectral solar irradiance with a classification of the single days into those with events and non-events. Furthermore, we have included half hour average values of number concentrations of different particle size ranges (size ranges: 3–5 nm, 3–6 nm, 3–10 nm and 3–50 nm). We have calculated correlation coefficients between the number concentration of the particles and the irradiance in the different wavelength groups for every day of the two years. The results with the highest correlations are those, which use a particle size of 3–10 nm. The differences in the correlation coefficients between the smaller size ranges and the 3–10 nm range is negligible (< 0.02). It could be due to the fact that at this small range 3–5 nm or 3–6 nm we are measuring particles at the detection limit of the DMPS system. So our results are more reliable if larger particles such as 3 to 10 nm were included for the following discussion. The size range 3 to 50 nm also includes the Aitken mode aerosols and here the correlation coefficients reach only half the previous values. This may be due to the fact that in this size range beside condensational growth, coagulation plays an important role and the influence of solar radiation is less important.

Figure 6 gives the average correlation coefficients between the number concentrations of particles between 3 and 10 nm and the spectral solar irradiance for the different classes in a histogram plot. The solid lines in each subplot mark the maximum value of the correlation coefficient in each class. The number of measured days per class is included in each subplot. All of the three event classes (A, B and C) have the highest correlation in the wavelength groups 3–5, which corresponds to the short wavelength range between 300–329 nm. After 330 nm the gaps between the solid lines and the bars in the first three subplots increase slightly towards higher wavelengths and reach a maximum around 30% at 580 nm. The absolute values of the correlation coefficients are not very high (around 0.6 for A-events) but we have to remember that these numbers are averages over all events per class and that in this context more than for the absolute values, the differences of the correlation coefficients between the single wavelength groups are interesting.

3.3 Case study for 5 May 2002

We will use now an example-day (5 May 2000) and present reasons for the higher correlation coefficients of the short wavelength bands. In order to do this we plotted the daily particle number concentrations for particles (3–10 nm),

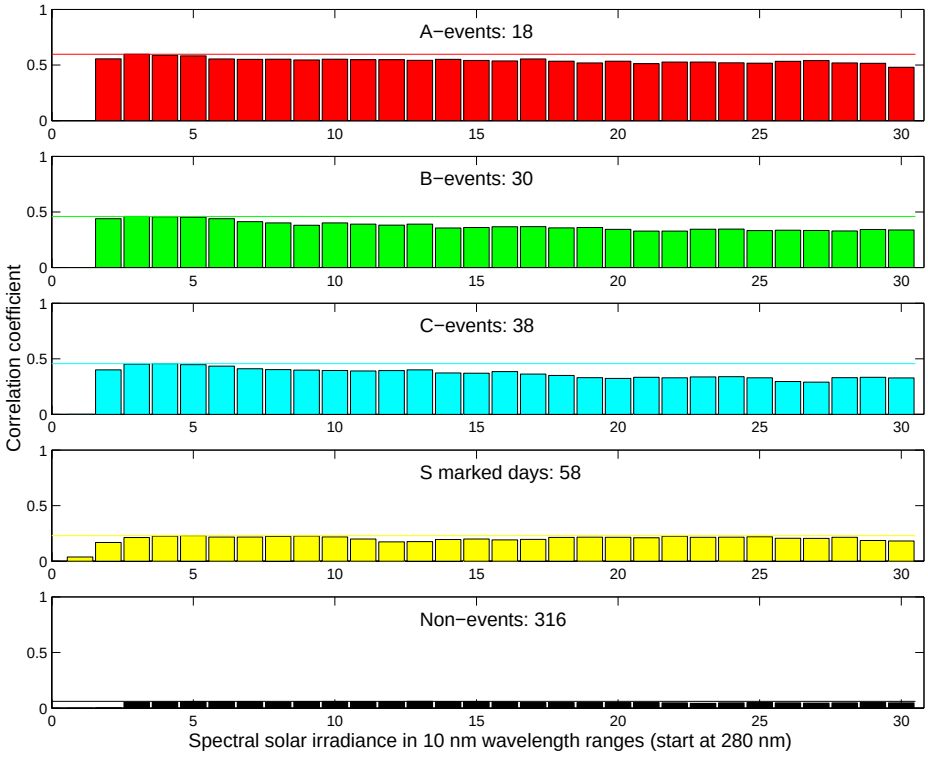

Fig. 6. Correlation coefficients for event classes between the number concentration of particles (3–10 nm) and the wavelengths groups from Eq. (1) ($I_{S,G}$).

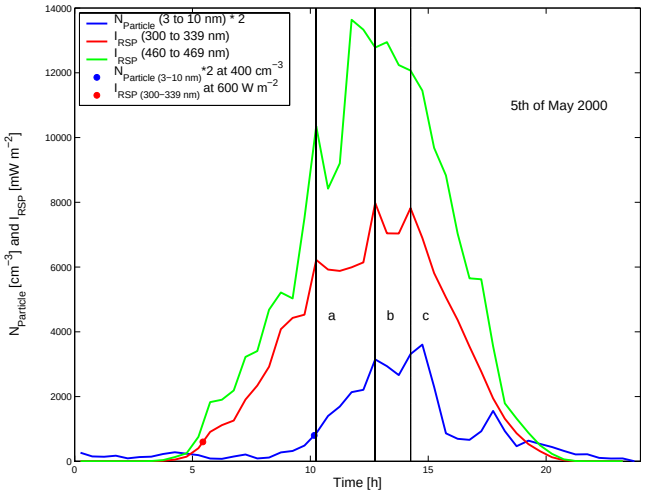

Fig. 7. Daily pattern of spectral solar irradiance and number concentration of particles for 5 May 2000.

short (300–339 nm) and longer wavelength irradiance (460–469 nm) in Fig. 7. The graph firstly shows that longer wavelength irradiances start to increase earlier as shorter (green compared to red curve). This is a physically well-known effect and because particle bursts always appear after sunrise and stop mostly long before sunset (see Table 1) this leads to higher correlation coefficients between UV solar radiation and the particle number concentrations. The second reason for the higher coefficients can be explained by the three peaks in the short wavelength irradiance curve marked by black lines (a, b and c). The irradiance peaks at line (a) and (c) in the morning and in the afternoon also appear in the particle curve during the next hour. The peak at line (b) around noon has no time lag and occurs at the same time in the radiation and particle concentration. Such patterns of solar radiation and particle number concentration curves occur on many event days. Most times the particles trends and peaks better fit the shorter wavelength of the solar spectrum by having the smallest time lags between peaks around noon when the pathways for the solar beam through the atmosphere reach their minima. However there are still event days where the correlation is quite small, but before making any conclusions we should consider two important facts:

– The radiospectrometer and the DMPS system are about 200 m apart from each other and the influence of moving clouds are not negligible for the solar irradiance at this distance.

– For both data sets (spectral irradiance and particles) half hour average values were used. A time step is necessary for handling all the data in reasonable computer time,

however many interested features of the daily trend are neglected.

3.4 Time lag between irradiance and particle increases

At the end of this session we use for each parameter – short wavelength radiation and particle concentration – one selected value to calculate the time difference between the two curves. For the particle we took the time when the concentration exceeds 400 particles cm^{-3} (blue dot in Fig. 7) and for the irradiance we chose 600 $mW\,m^{-2}$ (red dot in Fig. 7). The chosen values for irradiance and number concentration of particles are subjective selections for the situation in Hyytiälä, Finland and are not competitative for other locations. Figure 8 shows for all A- and B-event days for both parameters the specified times and the time lack (see also Table 1). There is a trend – especially in 2001 – that the time differences (green dots) with values around 0.5–2 h are smaller in winter till the beginning of spring than in summer and autumn (2–7 h). However, for the first event day on 5 February the particle concentration exceeds already two hours earlier the amount of 400 particles cm^{-3} before the irradiance reaches 600 $mW\,m^{-2}$. A more detailed analysis of different parameters of this day showed that on 5 February the highest ozone concentrations (39 ppb) between 1 January till 11 March were measured and that the concentration of H_2O was as small as 10^{17} molecules cm^{-3}. Further biological activity measured by CO_2 flux measurements in chambers were going on at this day. Bonn et al. (2002) investigated in laboratory experiments the highest ozonolysis-rates of monoterpenes and special of exocyclic monoterpenes (β-pinene and sabinene) for low water vapour and high ozone concentrations. Exactly this physical situation can be seen on day 36 of 2000. This feature and the results above indicate that there are most probably different chemical and photochemical mechanisms responsible for the production of the condensable vapour/s. From the high conformity between the short wavelength spectrum and the particles it appears that radiation leads to the formation of new aerosols on many event days, however, on other event days different mechanisms such as the ozonolysis of monoterpenes seem to be more important.

4 A potential mechanism explaining the indirect influence of short wavelength irradiance on the formation of SOA

In the previous session we showed that the short wavelengths range between 300 and 330 or 340 nm seems to be the most important spectral solar radiation band concerning the formation of new particles or the growth of new clusters to the detectable 3 nm size. In this session we will continue with this result and present a photochemical reaction mechanisms, as a hypothesis explaining the possible indirect influence of short

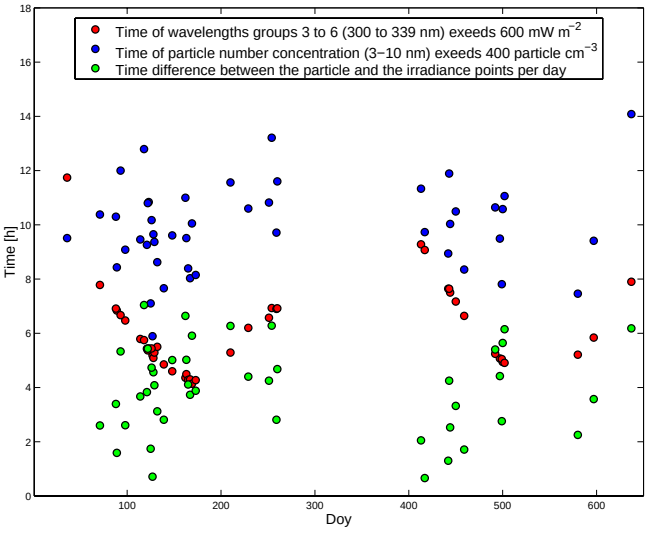

Fig. 8. Time short wavelength irradiance (300–339 nm) exceeds 600 $mW\,m^{-2}$ and particle number concentration (3–10 nm) exceeds 400 particle cm^{-3} for A- and B-events of 2000 and 2001. Further the difference between the two explained time points are included.

wavelength irradiance on the production of newly formed SOA. This is only one out of possible many different mechanisms participating in the formation of aerosols and the reason for presenting it here was to show one way besides any other photochemical reactions or the onset of vertical fluxes how solar irradiance and specially short wavelength irradiance can influence the formation of SOA.

First we calculate with the radiospectrometer data (average values of 5 nm ranges) between 280 and 350 nm for every half hour and day the average number of photons per 5 nm intervals.

$$Pho(k,h,j) = \frac{I_{SPR}(k,h,j) * WL(k)}{h * (c_o)} \quad (7)$$

with $WL(k)$ the wavelength per group (= 282.5, 287.5,. . ., 347.5 nm), h the Planck constant and c_o the speed of light in a vacuum. Further we include half hour average data for ozone and temperature in our analyses and calculate with the absorption cross section (ACS_{O3} – Molina and Molina, 1986) and the quantum yield (Q_{O3} – JPL publication 00-003, 2000) of ozone the photolyse rate for O_3 at the same times as in Eq. (7).

$$PR_{O3}(k,h,j) = Pho(k,h,j) \cdot Q_{O3}(k,T) \cdot ACS_{O3}(k) \quad (8)$$

With the photolyse rate and the half hour average values of ozone we now calculate in Eq. (9) the production rate of $O(^1D)$ as a function of time and wavelength

$$O(^1D)(k,h,j) = PR_{O3}(k,h,j) \cdot O_3(h,j) \quad (9)$$

Figure 8 shows as an example the production rate of $O(^1D)$ for 15 May 2000. In the x-axis a maximum occurs around

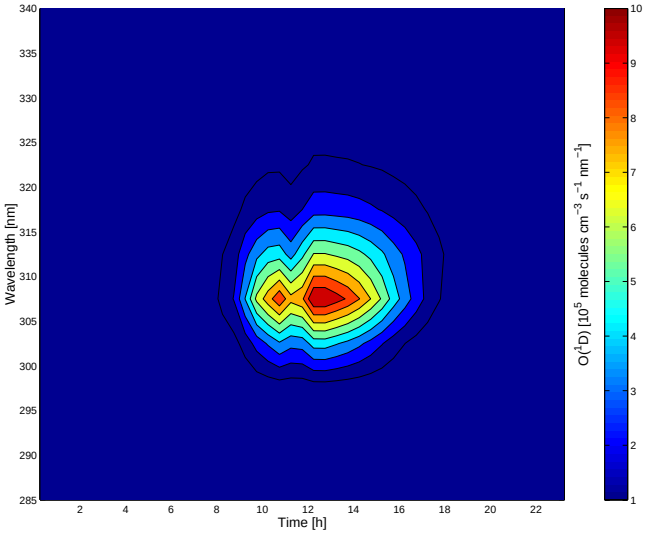

Fig. 9. Production rate of excited oxygen for 28 May 2000.

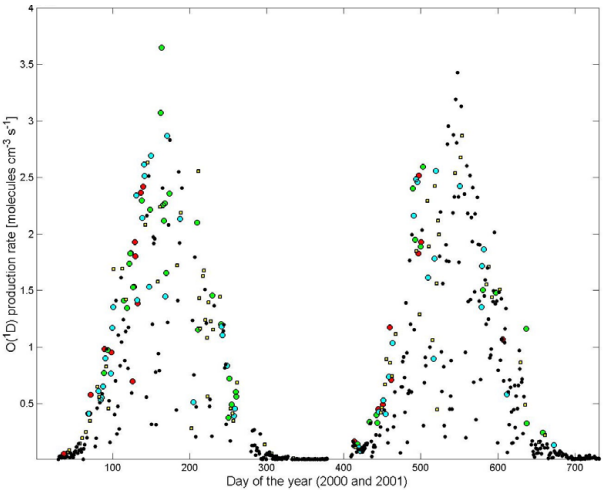

Fig. 10. Daily maxima production rate of excited oxygen for 2000 and 2001.

noon when the solar zenith angle has its minimum and in the *y*-axis a maximum occurs around 310 nm with a gradient of one magnitude in less than 15 nm in both directions. The maximum in the *y*-axis is a combination between the decreasing of the absorption cross-section and the quantum yield of ozone with higher wavelengths on one side and the steep increase of the spectral irradiance in the same direction on the other side. Although the absolute values of solar irradiance in the wavelength range from 300–330 nm is one to two magnitudes smaller than the maximum values between 450–500 nm this spectral solar band is the only one which enables the production of excited oxygen radicals in the troposphere. The produced $O(^1D)$ most often collides with N_2 and O_2, removing its excess energy and quenching back to its ground state by

$$O(^1D) + M \rightarrow O + M \quad (10)$$

Then the oxygen atom reacts with O_2 to replenish O_3. Occasionally, as much as every tenth $O(^1D)$ radical collides with H_2O and produces two hydroxyl radicals,

$$O(^1D) + H_2O \rightarrow 2OH \quad (11)$$

Two OH radicals are formed in Eq. (11) and this leads to an OH yield of approximately 0.2 molecule OH per O_3 molecule photolysed at a relative humidity of 50% and a temperature of 298 K (Seinfeld and Pandis, 1998). Hydroxyl radicals do not react with the major constituents of the atmosphere (N_2, O_2, CO_2 and H_2O). It is still an open question, which species and what kind of chemical reactions are responsible for the production of the condensable vapours involved in the formation of new aerosols. However, there is a high possibility that excited oxygen atoms and hydroxyl radicals are involved in these reactions. We will close this session with a temporally more comprehensive view on the explored theory by calculating the maxima of $O(^1D)$ production per day and plot these data for the whole year in Fig. 9. Most of the event days and especially the events in winter show very high values for excited oxygen production rate compared to the none-event days in the same month. However, there are still many none-event days with high values for this parameter; but it is well known that besides radiation other variables like the condensational sink, the temperature and the concentration of some till now unknown precursor species also influence the formation process of new aerosols.

5 Summary and conclusions

We analysed two years of solar spectral irradiance data and number concentrations of particles in different size ranges. It has been showed for the classification in events and non-events that there exists an increase in short wavelength solar radiation on event days. By normalising all daily average spectral radiation curves with the mean value of 330–380 nm, calculating ratios between the normalised values of events to the reference curve for all days of the two years or to reference curves for all days of the corresponding month respectively, we obtained the following results: The short wavelength irradiance between 300 and 340 nm on many event days in autumn and winter shows an increase compared to the reference curve for the corresponding month. During the rest of the year this trend disappears, however the absolute amounts of solar irradiance in this range is still as much as one magnitude higher in spring and summer. Using the same normalised values as before and calculating the ratios of the average of the different event classes to the reference curve of the two years we found a peak between 1.17 and 1.6 in the short wavelength range for all classes (Fig. 5) and a weak continuous increase towards higher wavelengths.

Furthermore we calculated for every day the correlation coefficients between number concentrations of particles (3–10 nm) and the different wavelengths groups. The graphs showed the same results as above with the highest correlation for the short wavelength range being between 300 and 330 nm. A more specific answer to the reasons for the differences in the correlation coefficients was given by using an example day (5 May 2000). Plotting the curves for particle number concentration and the spectral irradiance for short (300–339 nm) and longer (460–469 nm) wavelengths brought two aspects into focus. First, a temporal later increases of shorter wavelengths and second a higher agreement on most event days between the peaks of the particle curves and the peaks of the short wavelengths groups. The first effect is a well known physically aspect and it is attributed to the fact that particle bursts always occur after the sunrise and vanish long before sunset. The second point indeed more indicates a direct influence of the short wavelength solar spectrum on the formation of newly formed aerosols. Further we plotted the time differences when the solar radiation (300–339 nm) exceeds a value of 600 mW m^{-2} and the particle number concentration increases to 400 particles cm^{-3}. The results showed smaller time lags in winter and spring compared to summer and autumn with one day 5 February where the particle number concentration exceeded the selected value already two hours earlier than the irradiance. However this day also had the highest ozone concentration during winter (39 ppb), a very low amount of water vapour ($< 10^{17}$ molecules cm^{-3}) and biological activities. Bonn et al. (2002) found in laboratory experiments that ozonolysis of monoterpenes had the highest rates at small concentrations of H_2O and high concentrations of ozone. All conditions were present on 5 February. This indicates that during special periods different chemical and photochemical mechanisms are responsible for the production of condensable vapours and so for the formation of new aerosols.

In session 4 we presented a hypothesis to explain how the evaluated part of solar irradiance affects the production of condensable vapours and so the formation of new aerosols. For this reason we used half hour average values of ozone and temperature to calculate the production rate of excited oxygen atoms. The results of this analysis showed a maxima of $O(^1D)$ around noon and at 310 nm with a decrease of more than one magnitude below or above 295 and 325 nm, respectively. $O(^1D)$ is the main source in the troposphere for the production of hydroxyl radicals and the above introduced part of the solar spectrum is the only way to produce excited oxygen atoms in the troposphere. OH radicals are the most reactive species in the troposphere steering many atmospheric chemical reactions and could also be involved in the formation of new particles through chemical reactions, which produce the condensable vapours.

We conclude this publication with a correction concerning our last paper (Boy and Kulmala, 2002). As mentioned in the introduction we suggested in that paper UV-A to be the responsible solar radiation parameter for the formation of new aerosols by using a data set of different radiation sensors for 1999. Comparing the UV sensors data of 2000 and 2001 with the calculated UV radiospectrometer data we realised that UV-A measurements of the sensor were continuously approximately 10% too high and UV-B showed a strong dependency on the solar zenith angle. It is not possible afterwards to find the reasons for the overestimation of UV-A by the sensor, however a possible explanation could be the expanding of the sensor-filter (normally from 320–400 nm) into the UV-B range. This would explain the higher amounts of UV-A compared to other solar measurements during the time of the particle bursts, which occurred in 1999 and agree completely with the results of the present work.

References

Birmili, W., Berresheim, H., Plass-Duelmer, C., Elste, T., Gilge, S., Wiedensohler, A., and Uhrner, U.: The Hohenpeissenberg Aerosol Formation Experiment (HAFEX): A long-term study including size-resolved aerosol, H_2SO_4, OH, and monoterpenes measurements, Atmos. Chem. Phys. Discuss., 2, 1655–1697, 2001.

Birmili, W. and Wiedensohler, A.: New particle formation in the continental boundary layer: Meteorological and gas phase parameter influence, Geophys. Res. Letts., 27, 3325–3328, 2000.

Bonn, B., Schuster, G., and Moortgat, G. K.: Influence of water vapor on the process of new particle formation during monoterpene ozonolysis, J. Phys. Chem. A, 106 (12), 2869–2881, 2002.

Boy, M. and Kulmala, K.: Nucleation events in the continental boundary layer: Influence of physical and meteorological parameters, Atmos. Chem. Phys., 2, 1–16, 2002.

Clarke, A. D.: Atmospheric nuclei in Pacific midtroposphere: Their nature, concentration and evolution, J. Geophys. Res., 98, 20 633–20 647, 1993.

Clement, C. F., Pirjola, L., Dal Maso, M., Mäkelä, J. M., and Kulmala, M.: Analysis of particle formation bursts observed in Finland, J. Aerosol. Sci., 31, 2000.

Houghton, J. T., Meira Filho, L. G., Callander, B. A., Harris, N., Kattenburg, A., and Maskell, K.: Climate change 1995, Cambridge University Press, Cambridge, 1996.

Jokinen, V. and Mäkelä, J. M.: Closed loop arrangement with critical orifice for DMA sheath/excess flow system, J. Aerosol Sci., 28, 643–648, 1997.

JPL Publication 00-003, National Aeronautics and Space Administration, 2000.

Korhonen, P., Kulmala, M., Laaksonen, A., Viisanen, Y., McGraw, R., and Seinfeld, J. H.: Ternary nucleation of H_2SO_4, NH_3 and H_2O in the atmosphere, J. Geophys. Res., 104, 26 349–26 353, 1999.

Kulmala, M., Dal Maso, M., Mäkelä, J. M., Pirjola, L., Väkevä, M., Aalto, P., Miikkulainen, P., Hämeri, K., and O'Dowd, C.: On the formation, growth and composition of nucleation mode particles, Tellus B, 53, 479–490, 2001a.

Kulmala, M., Hämeri, K. K., Aalto, P., Mäkelä, J., Pirjola, L., Nilsson, E. D., Buzorius, G. Rannik, Ü., Dal Maso, M., Seidl, W., Hoffmann, T., Jansson, R., Hansson, H.-C. O'Dowd, C., and

Viisane, C.: Overview of the international project on biogenic aerosol formation in the boreal forest (BIOFOR), Tellus B, 53, 324–343, 2001b.

Kulmala, M., Pirjola, L., and Mäkelä, J. M.: Stable sulphate clusters as a source of new atmospheric particles, Nature, 404, 66–69, 2000.

Kulmala, M., Toivonen, A., Mäkelä, J. M., and Laaksonen, A.: Analysis of the growth of nucleation mode particles in Boreal Forest, Tellus, 50, 449–462, 1998.

Molina, L. T. and Molina, M. J.: Absolute absorption cross sections of ozone in the 185–350 nm wavelength range, J. Geophys. Res., 91, 14 501–14 508, 1986.

Mäkelä, J. M., Aalto, P., Jokinen, V., Pohja, T., Nissinen, A., Palmroth, S., Markkanen, T., Seitsonen, K., Lihavainen, H., and Kulmala, M.: Observations of ultrafine aerosol particle formation and growth in boreal forest, Geophys. Res. Lett., 24, 1219–1222, 1997.

Mäkelä, J. M., Dal Maso, M., Pirjola, L., Keronen, P., Laakso, L., and Kulmala, M.: Characteristics of the aerosol particle formation events observed at a boreal forest site in southern Finland, Boreal Env. Res., 5, 299–313, 2000.

Nilsson, E. D., Paatero, J., and Boy, M.: Effects of air masses and synoptic weather on aerosol formation in the continental boundary layer, Tellus, 53B, 2001.

O'Dowd, C. D., Geever, M., Hill, M. K., Smith, M. H., and Jennings, S. G.: New particle formation: Nucleation rates and spatial scales in the clean marine coastal environment, Geophys. Res. Letts., 25, 1661–1664, 1998.

Raes, F., Van Dingenen, R., Cuevas, E., Van Velthoven, P. F. J., and Prospero, J. M.: Observations of aerosols in the free troposphere and marine boundary layer of the subtropical Northeast Atlantic: Discussion of processes determining their size distribution, J. Geophys. Res., 102, 21 315–21 328, 1997.

Seinfeld, J. H.: Atmospheric Chemistry and Physics of Air Pollution, John Wiley & Sons, New York, 1998.

Weber, R. J., McMurry, P. H., Mauldin, L., Tanner, D. J., Eisele, F. L., Brechtel, F. J., Kreidenweis, S. M., Kok, G. L., Schilawski, R. D., and Baumgardner, D.: A study of new particle formation and growth involving biogenic and trace gas species measured during ACE 1, J. Geophys. Res., 103, 16 385–16 396, 1998.

Weber, R. J., McMurry, P. H., Mauldin, R. L., Tanner, D., Eisele, F. L., Clarke, A. D., and Kapustin, V.: New particle formation in the remote troposphere: A comparison of observations at various sites, Geophys. Res. Letts., 26, 307–310, 1999.

Vesala, T. E. A.: Long-term field measurements of atmospheresurface interactions in boreal forest combiding forest ecology, micrometeorology, aerosol physics and atmospheric chemistry, Trends Heat Mass Momentum Transf., 4, 17–35, 1998.